High-Resolution Solution Structure of Basic Fibroblast Growth Factor Determined by Multidimensional Heteronuclear Magnetic Resonance Spectroscopy‡

Franklin J. Moy,§ Andrew P. Seddon,||,⊥ Peter Böhlen,||,# and Robert Powers*,§

Departments of Structural Biology and Protein Chemistry, Wyeth-Ayerst Research, Pearl River, New York 10965

Received May 28, 1996; Revised Manuscript Received August 7, 1996⊗

ABSTRACT: The high-resolution solution structure of recombinant human basic fibroblast growth factor (FGF-2), a protein of 17.2 kDa that exhibits a variety of functions related to cell growth and differentiation, has been determined using three-dimensional heteronuclear NMR spectroscopy. A total of 30 structures were calculated by means of hybrid distance geometry−simulated annealing using a total of 2865 experimental NMR restraints, consisting of 2486 approximate interproton distance restraints, 50 distance restraints for 25 backbone hydrogen bonds, and 329 torsion angle restraints. The atomic rms distribution about the mean coordinate positions for the 30 structures for residues 29−152 is 0.43 ± 0.03 Å for the backbone atoms, 0.83 ± 0.05 Å for all atoms, and 0.51 ± 0.04 Å for all atoms excluding disordered side chains. The overall structure of FGF-2 consists of 11 extended antiparallel β-strands arranged in three groups of three or four strands connected by tight turns and loop regions creating a pseudo-3-fold symmetry. Two strands from each group come together to form a β-sheet barrel of six antiparallel β-strands. A helix-like structure was observed for residues 131−136, which is part of the heparin binding site (residues 128−138). The discovery of the helix-like region in the primary heparin binding site instead of the β-strand conformation described in the X-ray structures may have important implications in understanding the nature of heparin−FGF-2 interactions. A total of seven tightly bound water molecules were found in the FGF-2 structure, two of which are located in the heparin binding site. The first 28 N-terminal residues appear to be disordered, which is consistent with previous X-ray structures. A best fit superposition of the NMR structure of FGF-2 with the 1.9 Å resolution X-ray structure by Zhu et al. (1991) yields a backbone atomic rms difference of 0.94 Å, indicative of a close similarity between the NMR and X-ray structures.

Basic fibroblast growth factor (FGF-2),[1] a member of a protein family that includes three oncogenes (FGF-3, FGF-4, and FGF-5), exhibits angiogenic and a variety of growth and differentiation activities (Folkman & Klagsbrun, 1987; Baird & Bohlen, 1990; Basilico & Moscatelli, 1992; Miyamoto et al., 1993). Its diverse role in regulating cell growth and differentiation has suggested an involvement in wound healing, tumor growth, and cancer (Basilico & Moscatelli, 1992). A common feature of the FGF family members is their high affinity toward heparin sulfate proteoglycans (HSPG) (Miyamoto et al., 1993). The interaction of FGF-2 with HSPG is required for high-affinity binding to its cell surface tyrosine kinase receptor (FGFR) and is essential for mediating internalization and intracellular targeting through a proposed mechanism of receptor dimerization (Yayon et al., 1991; Roghani & Moscatelli, 1992; Reiland & Rapraeger, 1993; Pantoliano et al., 1994). It has been suggested that HSPG might interact directly with FGFR to facilitate the formation of a trimolecular complex and that the HSPG induced dimerization of FGF-2 may be important for receptor dimerization (Ornitz et al., 1992; Kan et al., 1993).

In order to better understand the mode of action of FGF-2 and in particular its interaction with HSPG and its cell surface receptor, we initiated a structural program to determine the three-dimensional structure of FGF-2 in solution by NMR spectroscopy. Previously (Moy et al., 1995), we reported the nearly complete ^{1}H, ^{15}N, ^{13}CO, and ^{13}C assignments and solution secondary structure for FGF-2. Here we present the determination of a high-resolution solution structure of FGF-2 using three-dimensional heteronuclear NMR spectroscopy. The resulting structure is based on a total of 2865 experimental NMR restraints, and the atomic rms distribution about the mean coordinate position for residues 29−152 is 0.43 ± 0.03 Å for the backbone atoms and 0.83 ± 0.05 Å for all atoms. A comparison with the 1.9 Å resolution X-ray structure by Zhu et al. (1991) indicates an overall similarity between the X-ray and NMR structures.

MATERIALS AND METHODS

NMR Sample Preparation. Uniformly (>95%) ^{15}N- and ^{15}N/^{13}C-labeled human recombinant FGF-2 was expressed in *Escherichia coli* and purified as described previously (Seddon et al., 1991; Moy et al., 1995). Numbering for

‡ Atomic coordinates for the 30 final simulated annealing structures (1BLD) and the restrained minimized mean structure (1BLA) of FGF-2 have been deposited in the Brookhaven Protein Data Bank.

* To whom correspondence should be addressed.

§ Department of Structural Biology.

|| Department of Protein Chemistry.

⊥ Current address: Department of Molecular Sciences, Pfizer, Inc., Groton, CT 06340.

Current address: ImClone System, Inc., New York, NY 10014.

⊗ Abstract published in *Advance ACS Abstracts,* October 1, 1996.

[1] Abbreviations: FGF-2 , basic fibroblast growth factor; FGFR, fibroblast growth factor tyrosine kinase receptor; HSPG, heparin sulfate proteoglycans; SOS, sucrose octasulfate; NMR, nuclear magnetic resonance; 3D, three dimensional; HSQC, heteronuclear single-quantum coherence spectroscopy; HMQC, heteronuclear multiple-quantum coherence spectroscopy; TPPI, time-proportional phase incrementation; NOE, nuclear Overhauser effect; NOESY, nuclear Overhauser enhanced spectroscopy.

S0006-2960(96)01260-3 CCC: $12.00

Table 1: Acquisition Parameters for NMR Experiments on FGF-2

	nucleus			no. of complex points			spectral width (ppm)			reference (ppm)		
experiment	F_1	F_2	F_3	F_1	F_2	F_3	F_1	F_2	F_3	F_1	F_2	F_3
HACAHB-COSY	^{1}H	^{13}C	^{1}H	54	12	512	7.57	14.3	12.07	4.75	46.0	4.75
long-range CCJ	^{13}C	^{13}C	^{1}H	128	14	256	87.2	3.66	8.00	30.0	30.0	2.65
coupled HCACO	^{13}C	^{13}C	^{1}H	15	96	512	15.06	12.0	8.42	54.0	175.0	4.75
HNHB	^{1}H	^{15}N	^{1}H	86	32	512	10.0	27.0	13.44	4.75	117.5	4.75
HNHA	^{1}H	^{15}N	^{1}H	48	48	512	9.50	27.0	13.44	4.75	117.5	4.75
^{15}N-edited ROESY	^{1}H	^{15}N	^{1}H	128	32	512	13.44	27.0	13.44	4.75	117.5	4.75
^{15}N-edited NOESY	^{1}H	^{15}N	^{1}H	128	32	512	13.44	27.0	13.44	4.75	117.5	4.75
^{13}C-edited NOESY	^{1}H	^{13}C	^{1}H	128	32	512	9.16	20.7	13.44	4.0	64.0	4.75

FGF-2 is from amino acid residue 1 deduced from the cDNA sequence encoding the 155-residue form. The mature form comprises residues 2−155. In addition, the two surface-exposed cysteines at positions 78 and 96 were changed to serines by site-directed mutagenesis to avoid unwanted intermolecular disulfide bond formation. C78S,C96S-FGF-2 has been shown to be as active as wild-type FGF-2 (Seddon et al., 1991). Samples for NMR contained 1 mM ^{15}N- or ^{15}N/^{13}C-labeled FGF-2, pH 5.5, dissolved in a buffer containing 50 mM potassium phosphate, 2 mM NaN_3, and 10 mM deuterated DTT in either 90% H_2O/10% D_2O or 100% D_2O.

NMR Data Collection. All spectra except the HACAHB-COSY experiment were recorded at 25 °C on a Bruker AMX600 spectrometer using a gradient-enhanced triple-resonance ^{1}H/^{13}C/^{15}N probe. The HACAHB-COSY experiment was recorded on a Varian Unity 600 spectrometer. For spectra recorded in H_2O, water suppression was achieved with the WATERGATE sequence and water−flip back pulses (Piotto et al., 1992; Grzesiek & Bax, 1993). Quadrature detection in the indirectly detected dimensions was recorded with the States−TPPI hypercomplex phase increment (Marion et al., 1989a) and collected when appropriate with refocusing delays to allow for spectra with 0, 0; +90, −180; or 180, −360 phase correction.

The present structure is based on the following series of spectra: HNHA (Vuister & Bax, 1993), HNHB (Archer et al., 1991), 3D long-range ^{13}C−^{13}C correlation (Bax et al., 1992), coupled CT-HCACO (Powers et al., 1991; Vuister et al., 1992), HACAHB-COSY (Grzesiek et al., 1995), 3D ^{15}N- (Marion et al., 1989b; Zuiderweg & Fesik, 1989) and ^{13}C-edited NOESY (Ikura et al., 1990; Zuiderweg et al., 1990), and ^{15}N-edited ROESY (Clore et al., 1990a). The ^{15}N-edited NOESY, ^{13}C-edited NOESY, and ^{15}N-edited ROESY experiments were collected with 100, 120, and 40 ms mixing times, respectively. Table 1 summarizes the acquisition parameters for each of the experiments used in determining the solution structure of FGF-2.

Spectra were processed using the NMRPipe software package (Delaglio et al., 1995) and analyzed with PIPP (Garrett et al., 1991) on a Sun Sparc Workstation. When appropriate, data processing included a solvent filter, zero-padding data to a power of 2, linear predicting back one data point of indirectly acquired data to obtain zero (zero and first order) phase corrections, and linear prediction of additional points for the indirectly acquired dimensions to increase resolution. Linear prediction by means of the mirror image technique was used only for constant-time experiments. In all cases data were processed with a skewed sine-bell apodization function, and one zero filling was used in all dimensions.

Interproton Distance Restraints. NOEs assigned from the 3D ^{15}N- and ^{13}C-edited NOESY experiments were classified into strong, medium, weak, and very weak corresponding to interproton distance restraints of 1.8−2.7 Å (1.8−2.9 Å for NOEs involving NH protons), 1.8−3.3 Å (1.8−3.5 Å for NOEs involving NH protons), 1.8−5.0 Å, and 1.8−6.0 Å, respectively (Williamson et al., 1985; Clore et al., 1986). Upper distance limits for distances involving methyl protons and nonstereospecifically assigned methylene protons were corrected appropriately for center averaging (Wuthrich et al., 1983), and an additional 0.5 Å was added to upper distance limits for NOEs involving methyl protons (Clore et al., 1987; Wagner et al., 1987). Hydrogen bond restraints were deduced on the basis of slowly exchanging NH protons which were identified by recording an HSQC spectrum 2 days after exchanging an FGF-2 sample from H_2O to D_2O. The corresponding H-bond acceptors were identified from the pattern of interstrand NOEs involving the NH and CαH protons and an initial set of structure calculations. Two distance restraints were used for each hydrogen bond (r_{NH-O} = 1.5−2.3 Å, r_{N-O} = 2.4−3.3 Å).

Torsion Angle Restraints and Stereospecific Assignments. The β-methylene stereospecific assignments and χ_1 torsion angle restraints were obtained primarily from a qualitative estimate of the magnitude of $^3J_{\alpha\beta}$ coupling constants from the HACAHB-COSY experiment (Grzesiek et al., 1995) and $^3J_{N\beta}$ coupling constants from the HNHB experiment (Archer et al., 1991). Further support for the assignments was obtained from approximate distance restraints for intraresidue NOEs involving NH, CαH, and CβH protons (Powers et al., 1993).

The ϕ and ψ torsion angle restraints were obtained from $^3J_{NH\alpha}$ coupling constants measured from the relative intensity of Hα cross peaks to the NH diagonal in the HNHA experiment (Vuister & Bax, 1993), from a qualitative estimate of the magnitude of $^3J_{\alpha\beta}$ coupling constants from the HACAHB-COSY experiment (Grzesiek et al., 1995), and from approximate distance restraints for intraresidue and sequential NOEs involving NH, CαH, and CβH protons by means of the conformational grid search program STEREOSEARCH (Nilges et al., 1990), as described previously (Kraulis et al., 1989). $^1J_{C\alpha H\alpha}$ coupling constants obtained from a coupled 3D CT-HCACO spectrum were used to ascertain the presence of non-glycine residues with positive ϕ backbone torsion angles (Vuister et al., 1992).

The Ile and Leu χ_2 torsion angle restraints and the stereospecific assignments for leucine methyl groups were determined from $^3J_{C\alpha C\delta}$ coupling constants obtained from the relative intensity of Cα and Cδ cross peaks in a 3D long-range ^{13}C−^{13}C NMR correlation spectrum (Bax et al., 1992), in conjunction with the relative intensities of intraresidue NOEs (Powers et al., 1993). Stereospecific assignments for valine methyl groups were determined on the basis of the relative intensity of intraresidue NH−CγH and CαH−CγH

NOEs as described by Zuiderweg et al. (1985). The minimum ranges employed for the ϕ, ψ, and χ torsion angle restraints were ±30°, ±50°, and ±20°, respectively (Kraulis et al., 1989).

Structure Calculations. The structures were calculated using the hybrid distance geometry−dynamical simulated annealing method of Nilges et al. (1988a) with minor modifications (Clore et al., 1990b) using the program X-PLOR (Brunger, 1993). The target function that is minimized during restrained minimization and simulated annealing contains only quadratic harmonic terms for covalent geometry, square-well quadratic potentials for the experimental distance and torsion angle restraints, and a quartic van der Waals term for nonbonded contacts. All peptide bonds were constrained to be planer and trans. There were no hydrogen-bonding, electrostatic, or 6−12 Lennard-Jones empirical potential energy terms in the target function.

The structure determination followed an iterative structure refinement procedure which has been previously described in detail (Clore & Gronenborn, 1991; Forman-Kay et al., 1991a; Powers et al., 1993). The approach is to incorporate more experimental restraints at each successive stage as the quality of the structures improves where the current structure is used to resolve ambiguities in the assignments of NOEs and to predict NOEs corresponding to short interproton distances which are then verified from experimental data. Since NOESY spectra were recorded with mixing times ranging from 100 to 120 ms, the classification of NOEs may be influenced by spin diffusion; therefore, NOE classifications were reevaluated on the basis of the observed distances and potential for spin-diffusion pathways in the current ensemble of structures. If a distance restraint was systematically violated in the ensemble of structures, the NOE was reclassified into the next class (i.e., from strong to medium or from medium to weak). At later stages in the refinement, it is possible to assign NOE distance restraints to CδH and CϵH of well-defined Phe and Tyr to only one side of the ring and assign a χ_2 torsion angle restraint.

Tightly Bound Water. The presence of seven tightly bound water molecules in the FGF-2 structure was identified from the 3D ^{15}N-edited ROESY spectrum by the observation of ROEs from the water frequency (4.75 ppm) to NH protons (Otting & Wuthrich, 1989; Clore et al., 1990a; Forman-Kay et al., 1991b; Clore & Gronenborn, 1992) (Figure 1). A number of other cross peaks were observed but could not be distinguished between an ROE to water or to a spatially close CαH or a rapidly exchanging group (e.g., the hydroxyl group of Ser or Thr). The tightly bound water molecules were identified after completion of the simulated annealing calculations and were not included in the refinement process but could be spatially accommodated in the FGF-2 structures as identified by the Protein Health module in Quanta 4.1 (Molecular Simulations Inc., San Diego).

The final 30 simulated annealing structures were calculated on the basis of 2865 experimental NMR restraints consisting of 2486 approximate interproton distance restraints, 50 distance restraints for 25 backbone hydrogen bonds, and 329 torsion angle restraints consisting of 118 ϕ, 99 ψ, 84 χ_1, and 28 χ_2 torsion angle restraints. Stereospecific assignments were obtained for 70 of the 109 residues with β-methylene protons, for the methyl groups of 5 of the 7 Val residues, and for the methyl groups of 10 of the 14 Leu residues. In addition, 6 out of the 8 Phe residues and 5 out of the 7 Tyr residues were well defined, making it possible to assign NOE restraints to only one of the pair of CδH and CϵH protons and to assign a χ_2 torsion angle restraint. Similarly, χ_2 torsion angle restraints were assigned to 2 out of 3 of the His residues and the lone Trp residue.

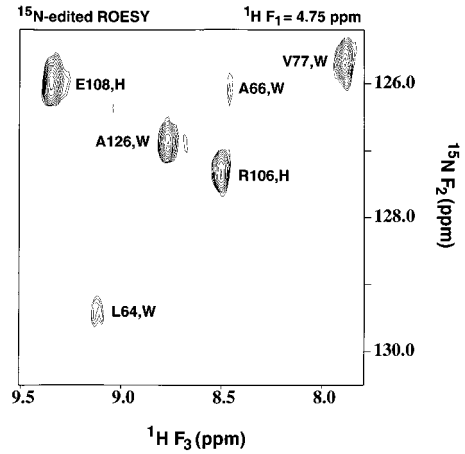

FIGURE 1: Expanded ^{15}N(F_2)−^{1}H(F_3) plane taken at the ^{1}H(F_1) frequency of water (4.75 ppm) of the 3D-edited ROESY spectrum of FGF-2. The ROE cross peaks to bound water are indicated by the letter W. ROE cross peaks whose origin could not be distinguished between a direct ROE with bound water or ROEs coupled to chemical exchange with water through a neighboring side-chain exchangeable group are indicated by the letter H.

RESULTS AND DISCUSSION

Converged Structures. A summary of the structural statistics for the final 30 simulated annealing ⟨SA⟩ structures of human FGF-2 is provided in Table 2, and best fit superpositions of the backbone atoms and selected side chains are shown in Figure 2. Residues 1−28 and 153−155 are disordered in the FGF-2 NMR structure and have been excluded from the statistical analysis. The atomic rms distribution of the 30 simulated annealing structures about the mean coordinate positions for residues 29−152 is 0.43 ± 0.03 Å for the backbone atoms, 0.83 ± 0.05 Å for all atoms, and 0.51 ± 0.04 Å for all atoms excluding disordered surface side chains (Table 3). The mean standard deviations for the ϕ and ψ backbone torsion angles of residues 29−152 are 10.9 ± 10.3° and 11.2 ± 9.3°, respectively. This is well within the minimum ranges allowed for the ϕ and ψ torsion angle restraints of ± 30° and ± 50°, respectively. This is consistent with empirical observations that the quality of the NMR structures is based primarily on the number and accuracy of the distance restraints and the presence of dihedral restraints primarily assists in the convergence rate of the simulated annealing calculations. The atomic rms distribution about the mean coordinate positions and the angular rms deviations for the ϕ, ψ, χ_1, and χ_2 torsion angles, together with the variations in surface accessibility, are also shown in Figure 3 as a function of residue number. The high quality of the FGF-2 NMR structure is also evident by the very small deviations from idealized covalent geometry, the lack of bad nonbonded contacts, and the absence of interproton distance and torsion angle violations greater than 0.1 Å and 1°, respectively (Table 2). Further support for the quality of the FGF-2 NMR structure is seen by the calculated values of two energy parameters not included in the target function for simulated annealing. Large negative values for the Lennard-Jones−van der Waals energy (−513 ± 13 kcal mol^{-1}) and for the solvation free energy of

Table 2: Structural Statistics and Atomic rms Differences[a]

(A) Structural Statistics

	⟨SA⟩	$(\overline{SA})_r$	X-ray[b]
rms deviations from exptl distance restraints (Å)[c]			
all (2536)	0.0036 ± 0.0019	0.0016	0.439
interresidue sequential ($\|i-j\|=i$) (648)	0.0040 ± 0.0039	0.0020	0.251
interresidue short range ($1<\|i-j\|\le 5$) (275)	0.0017 ± 0.0013	0.0010	0.594
interresidue long range ($\|i-j\|>5$) (918)	0.0023 ± 0.0016	0.0010	0.573
intraresidue (645)	0.0038 ± 0.0024	0.0000	0.161
H-bonds (50)[d]	0.0060 ± 0.0018	0.0050	0.099
rms deviation from exptl dihedral restraints (deg) (329)[c,e]	0.101 ± 0.056	0.054	26.3
F_{NOE} (kcal mol^{-1})[f]	2.12 ± 2.77	0.305	2655
F_{tor} (kcal mol^{-1})[f]	0.27 ± 0.41	0.058	5486
F_{repel} (kcal mol^{-1})[f]	18.49 ± 2.12	13.55	584
F_{L-J} (kcal mol^{-1})[g]	−513 ± 13	−529	−280
F_{SFE} (kcal mol^{-1})[h]	−141 ± 5	−155	−146
deviations from idealized covalent geometry			
bonds (Å) (2471)	0.002 ± 0	0.002	0.024
angles (deg) (4465)	0.525 ± 0.005	0.513	4.370
impropers (deg) (1299)[i]	0.266 ± 0.028	0.255	7.396
overall *G*-factor[j]	−0.088 ± 0.018	−0.05	−0.10

(B) Atomic rms Differences (Å)

	residues 29−152		secondary structure[k]		ordered side chain[l]
	backbone atoms	all atoms	backbone atoms	all atoms	all atoms
⟨SA⟩ vs $\overline{SA}$	0.43 ± 0.03	0.83 ± 0.05	0.39 ± 0.03	0.69 ± 0.06	0.51 ± 0.04
⟨SA⟩ vs $(\overline{SA})_r$	0.50 ± 0.04	0.95 ± 0.05	0.40 ± 0.05	0.81 ± 0.09	0.58 ± 0.05
$(\overline{SA})_r$ vs $\overline{SA}$	0.26	0.47	0.21	0.43	0.29
$\overline{SA}$ vs X-ray	0.93	1.31	0.76	1.15	1.25
$(\overline{SA})_r$ vs X-ray	0.94	1.41	0.78	1.24	1.29
⟨SA⟩ vs X-ray	1.03 ± 0.04	1.50 ± 0.04	0.83 ± 0.05	1.34 ± 0.05	1.35 ± 0.05

[a] The notation of the NMR structures is as follows: ⟨SA⟩ are the final 30 simulated annealing structures; $\overline{SA}$ is the mean structure obtained by averaging the coordinates of the individual SA structures best fit to each other (excluding residues 1−28 and 153−155); $(\overline{SA})_r$ is the restrained minimized mean structure obtained by restrained minimization of the mean structure $\overline{SA}$ (Nilges et al., 1988a). The number of terms for the various restraints is given in parentheses. [b] X-ray is the 1.9 Å resolution X-ray structure of Zhu et al. (1991). Tyr and Phe χ_2 dihedral angles in the X-ray structure were changed to be consistent with the NMR structure since it is not possible to differentiate between +90° or −90° in the X-ray structure. Without this correction, the calculation of F_{NOE} and F_{tor} would be artificially high for the X-ray structure. Residues 1−27 and 153−155 are not present, and residues 28, 55, 65, 67−69, 87, 85, 99, 119, 129, 133, and 144 have disordered side chains and only contain backbone atoms in the X-ray structure (residue numbering was corrected for the additional eight amino acids in the NMR sequence). [c] None of the structures exhibited distance violations greater than 0.1 Å or dihedral angle violations greater than 1°. [d] For the backbone NH−CO hydrogen bond there are two restraints: r_{NH-O} = 1.5−2.3 Å and r_{N-O} = 2.5−3.3 Å. All hydrogen bonds involve slowly exchanging NH protons. [e] The torsion angle restraints comprise 118 ϕ, 99 ψ, 84 χ_1, and 28 χ_2 restraints. [f] The values of the square-well NOE (F_{NOE}) and torsion angle (F_{tor}) potentials [cf. eqs 2 and 3 in Clore et al. (1986)] are calculated with force constants of 50 kcal mol^{-1} Å^{-2} and 200 kcal mol^{-1} rad^{-2}, respectively. The value of the quartic van der Waals repulsion term (F_{rep}) [cf. eq 5 in Nilges et al. (1988)] is calculated with a force constant of 4 kcal mol^{-1} Å^{-4} with the hard-sphere van der Waals radius set to 0.8 times the standard values used in the CHARMM (Brooks et al., 1983) empirical energy function (Nilges et al., 1988a−c). [g] E_{L-J} is the Lennard-Jones−van der Waals energy calculated with the CHARMM empirical energy function and is *not* included in the target function for simulated annealing or restrained minimization. [h] E_{SFE} is the calculated solvation free energy of folding (Eisenberg & McLachlan, 1986; Chiche et al., 1990) and is *not* included in the target function for simulated annealing or restrained minimization. The expected value of E_{SFE} for a protein the size of FGF-2 (154 residues) is −159 kcal mol^{-1} (Chiche et al., 1990). [i] The improper torsion restraints serve to maintain planarity and chirality. [j] The overall *G*-factor was calculated using the PROCHECk program (Laskowski et al., 1993). [k] The residues in the regular secondary structure are 31−34 (β_1), 39−43 (β_2), 49−53 (β_3), 62−67 (β_4), 71−76 (β_5), 81−85 (β_6), 91−94 (β_7), 103−107 (β_8), 113−117 (β_9), 124−126 (β_{10}), and 143−151 (β_{11}). [l] The disordered side chains that were excluded are as follows: residues 1−27; residues 153−155; Lys 30 from Cϵ; Arg 31 beyond Cδ; Lys 35 from Cδ; Arg 42 beyond Cδ; Arg 48 from Cδ; Glu 54 from Cγ; Lys 55 from Cβ; Ser 56 from Cβ; Asp 57 from Cβ; Lys 61 from Cδ; Gln 63 from Cδ; Gln 65 from Cγ; Glu 67 from Cβ; Glu 68 from Cγ; Arg 69 from Cβ; Lys 75 from Cϵ; Ser 78 beyond Cβ; Asn 80 beyond Cγ; Arg 81 beyond Cδ; Met 85 beyond Cγ; Lys 86 from Cδ; Glu 87 from Cβ; Arg 90 beyond Cδ; Ser 94 beyond Cγ; Lys 95 from Cδ; Ser 96 beyond Cγ; Val 97 beyond Cβ; Asp 99 from Cβ; Glu 100 from Cδ; Glu 105 from Cδ; Arg 106 from Cγ; Leu 107 from Cγ; Glu 108 from Cδ; Ser 109 from Cβ; Asn 110 from Cγ; Asn 111 beyond Cγ; Asn 113 beyond Cγ; Arg 116 from Cγ; Arg 118 beyond Cδ; Lys 119 from Cδ; Lys 128 from Cδ; Arg 129 from Cβ; Lys 134 from Cϵ; Lys 138 from Cδ; Gln 143 from Cδ; Lys 144 from Cδ; and Met 151 beyond Cγ.

unfolding (−141 ± 5 kcal mol^{-1}) are consistent with the structure of a properly folded protein. The solvation free energy of unfolding (F_{SFE}) initially appears to be slightly lower than expected for a protein the size of FGF-2, since the predicted F_{SFE} for a 154 residue protein is −159 kcal mol^{-1} (Eisenberg & McLachlan, 1986; Chiche et al., 1990). This lower than expected value for F_{SFE} is due to the fact that the first 28 N-terminal residues are ill-defined and do not properly contribute to the solvation free energy of unfolding. The F_{SFE} of −141 ± 5 kcal mol^{-1} calculated for residues 29−152 is greater than the predicted F_{SFE} of −125 kcal mol^{-1} for a 124-residue protein, indicating a properly folded protein with an appropriate distribution of hydrophobic and hydrophilic residues within the interior and exterior of the protein.

Most of the backbone torsion angles for non-glycine residues lie within expected regions of the Ramachandran plot (Figure 4). Seventy percent of the residues lie within the most favored region of the Ramachandran ϕ, ψ plot, 25% in the additionally allowed regions, and 4% in the generously allowed region. Most of the outlying residues correspond to the disordered N-terminal region of the protein. $^1J_{C\alpha H\alpha}$

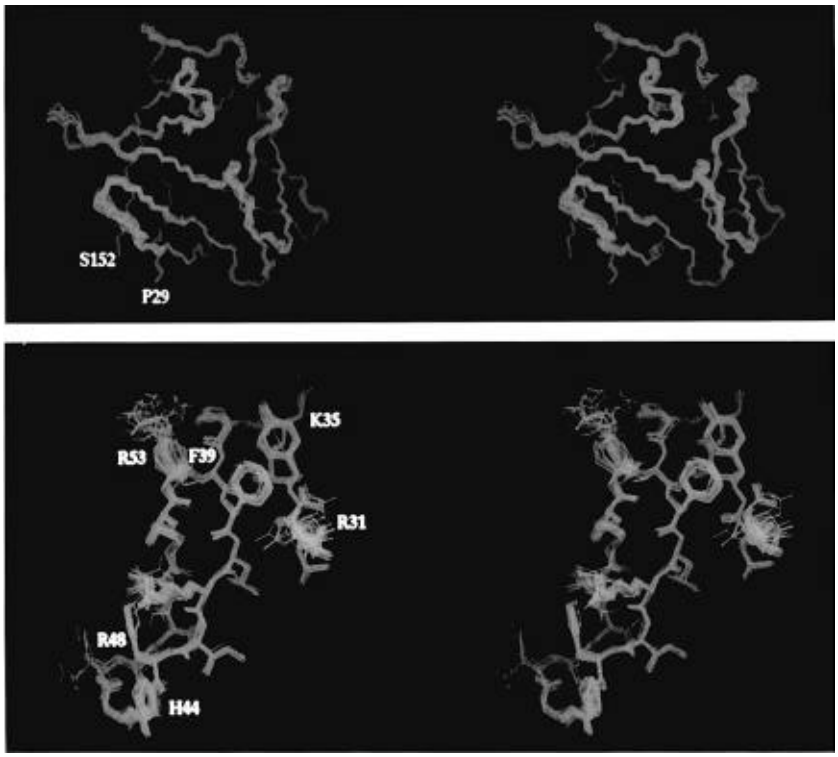

FIGURE 2: Stereoviews showing the best fit superpositions of (top) the backbone (N, Cα, C) and (bottom) all atoms of the 30 final simulated annealing structures. Residues 29−152 and 31−53 are shown in the top and bottom panels, respectively.

Table 3: Observed ROEs to Bound Water and Predicted Hydrogen Bonds

water	donor	acceptor	ROE
W1	Leu 64 NH	Asp 28 O	Leu 64 NH Ala 66 NH
W2	Leu 32 NH	Leu 41 O Ile 60 O	Leu 32 NH Leu 41 NH
W3	Ser 78 NH Lys 61 NH	Lys 61 O His 59 O	Ile 43 NH His 59 NH Arg 61 NH Val 77 NH
W4	Ile 74 NH	Leu 83 O	Leu 83 NH
W5	Arg 119 NH	Glu 100 O Phe 102 O	Met 85 NH Phe 102 NH
W6	Ala 126 NH	Lys 134 O	Ala 126 NH
W7	Gln 132 NH	Lys 128 O	Lys 128 NH

coupling constants from the coupled CT-HCACO experiment indicated that Asn 80 and Asn 111 both have positive ϕ torsion angles. Both residues are located at the end of a type I reverse turn and precede β-strands VI and IX, respectively. Presumably, the positive ϕ torsion angles allow for proper β-sheet formation upon completing the turn.

Description of the Structure. A ribbon diagram of the restrained minimized mean NMR structure, $(\overline{SA})_r$, of FGF-2 is depicted in Figure 5. The overall structure of FGF-2 is comprised of 11 extended antiparallel β-strands connected by tight turns and loop regions arranged in three β-sheets composed of three to four β-strands (β-sheet 1, I_{31-34}, II_{39-43}, III_{48-53}, $XII_{148-151}$; β-sheet 2, IV_{62-67}, V_{71-76}, VI_{81-85}, VII_{91-94}; β-sheet 3, $VIII_{103-107}$, $IX_{113-117}$, $X_{124-126}$). β-Strands I and II, β-strands II and III, and β-strands IV and V are connected by a type II reverse turn with Gly 37, Gly 47, and Gly 70 in the $i + 2$ position adopting a positive ϕ torsion angle, respectively. β-strands V and VI and β-strands VIII and IX are connected by a type I reverse turn while the remaining strands are connected by short or long loops. Examples of the type I and type II reverse turns observed in the FGF-2 NMR structure are shown in Figure 6. The resulting structure has a pseudo 3-fold axis of symmetry where two strands from each β-sheet are part of a six-stranded β-barrel structure. Based on the fact that FGF-2 was identified as a structural homolog of IL-1β, the FGF-2 NMR structure was expected to be composed of 12 β-strands (Eriksson et al., 1991; Zhang et al., 1991; Zhu et al., 1991). The "missing" β-strand (XI) corresponds to residues 131−136 which clearly adopt a helix-like conformation in the FGF-2 NMR structure (Moy et al., 1995). It is intriguing to note that residues 131−136 are part of the primary heparin binding site (128−138) and the unexpected helix-like conformation these residues adopt may be crucial for the binding of FGF-2 to heparin (Figure 7).

An unusual feature of the FGF-2 structure is the observation that the first 28 N-terminal residues are disordered and highly mobile as evident by small order parameters (Moy et al., unpublished). This disorder has also been attributed to a cis/trans isomerization for Pro 10 and Pro 13 (Moy et al., 1995). This is also consistent with the observation that the first 17−19 residues in the X-ray structures of FGF-2 (10−155) are not visible in the electron density map and have been identified as disordered (Zhu et al., 1983; Ago et al., 1991; Eriksson et al., 1991; Zhang et al., 1991). Clearly, the first 28 N-terminal residues do not play a role in the overall fold of the protein, and removal of these residues does not affect the activity of FGF-2 (Seddon et al., 1991).

The core of the protein is exclusively hydrophobic as indicated by the surface accessibility plot in Figure 3. Nevertheless, the presence of seven tightly bound water molecules (W1−W7) in the core of the protein was determined from ROEs between water backbone NHs observed in the 3D ^{15}N-edited ROESY spectrum (Figure 1). The 11 observed ROEs to bound water and the predicted

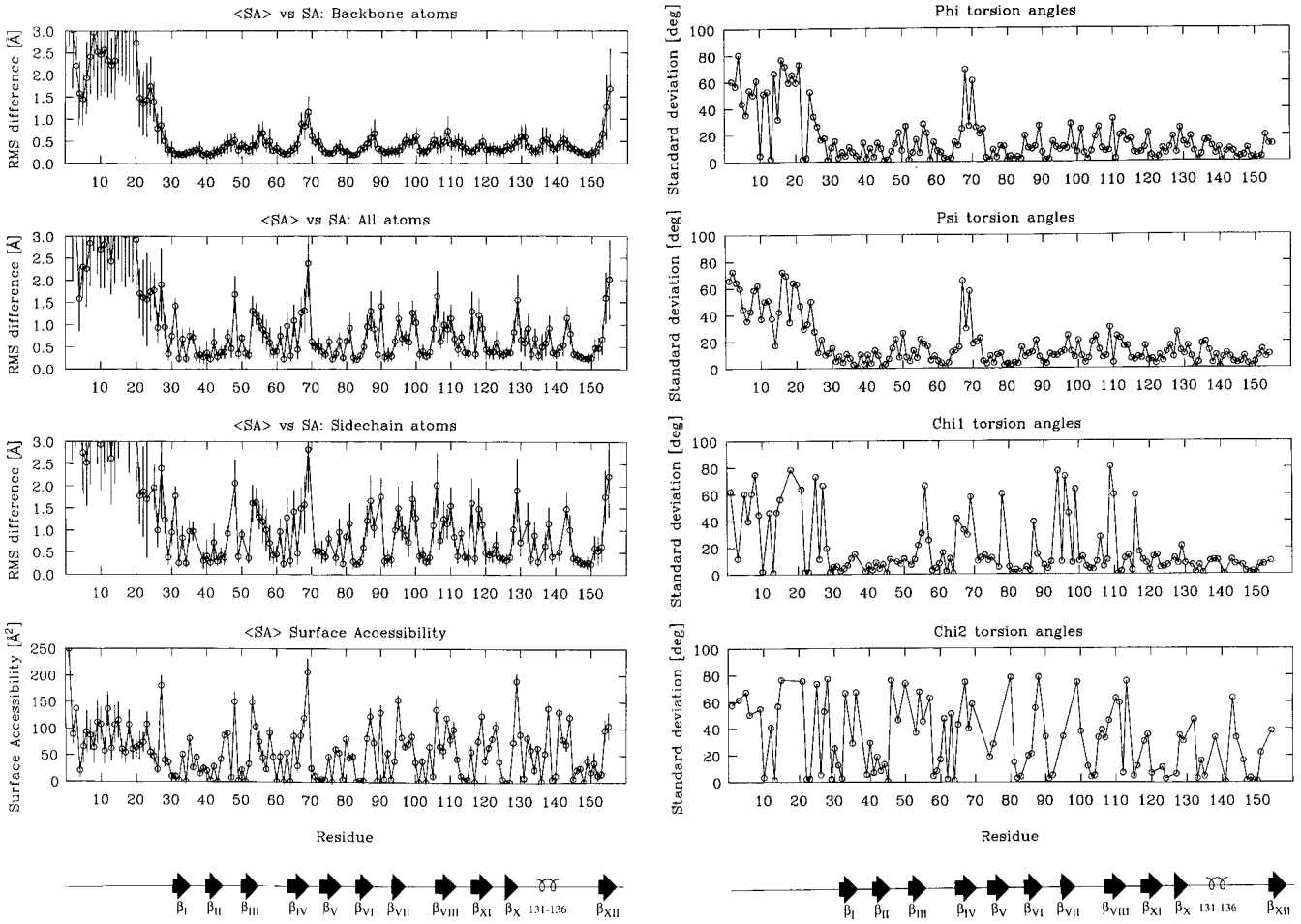

FIGURE 3: Atomic rms distribution of the 30 individual simulated annealing structures about the mean structure $\overline{SA}$ for the backbone (N, Cα, C, O) atoms, all atoms, and side-chain atoms as a function of residue number, together with the variation in surface accessibility of each residue (left). Standard deviation of the backbone ϕ and ψ and side-chain χ_1 and χ_2 torsion angles for the 30 simulated annealing structures as a function of residue number (right). The circles represent the average value at each residue, and the error bars indicate the standard deviations in these values. Error bars greater than 3 Å were truncated for clarity. The bottom of the figure presents a schematic diagram of the secondary structure of FGF-2, with β-strands shown as arrows.

hydrogen bond donors/acceptors with the bound water are listed in Table 3. The prediction of the hydrogen bond donors/acceptors was based on the close proximity of the observed ROEs in the FGF-2 structure and the presence of a structural "hole" in the structure determined by the Protein Health module in Quanta 4.1 (Molecular Simulations, Inc., San Diego). ROEs were also observed between W4 and Ile 74 NH and between W5 and Arg 119 NH, but both of these NHs are also in close proximity to a Ser OH group. Therefore, it was not possible to unambiguously assign these ROEs to an interaction with bound water; however, they are consistent with the placement of W4 and W5. The approximate placement of the seven bound waters is depicted in Figure 8. Clearly, the locations of the bound waters provide stability to the local structure. All the water molecules occur at either the beginning or end of a β-sheet where the β-strands begin to spread apart and the hydrogen bonding between the strands is lost. Thus, the presence of the water molecule restores this lost hydrogen bond interaction by acting as a bridge and forming hydrogen bonds to both of the strands. Water molecules W2, W3 and W4, W5 are located at a T-junction where the end of one β-sheet is perpendicular to another strand and provide additional stability by forming hydrogen bonds between all three strands. The presence of these structural water molecules in the NMR solution structure of FGF-2 is consistent with the observation of bound water in the crystal structures (Eriksson et al., 1991, 1993).

Examination of the minimized mean FGF-2 structure suggested the presence of five potential hydrogen bonds between surface side chains and backbone atoms. The presence of these hydrogen bonds suggests a role in stabilizing three reverse turns. Asn 36 is in the reverse turn between β-strands I and II; its side chain forms a potential hydrogen bond with the carbonyl of Lys 144 which is near β-strand XI and part of the β-sheet composed of β-strands I, II, and XI. Asp 46 is in the reverse turn between β-strands II and III; its side chain forms a potential hydrogen bond to the backbone NH of Arg 48. This reverse turn is further stabilized by the hydrogen bond between the side chain of Arg 81, which is part of β-strand VI, and the carbonyl of Pro 45. Asp 88 is part of the reverse turn between β-strands VI and VII and forms potential hydrogen bonds between its side chain and the NH of both Gly 89 and Arg 90.

Comparison of the Solution Structure of FGF-2 with the X-ray Structure. Refined X-ray structures for both wild-type and C78S,C96S-FGF-2 have been determined and shown to have nearly identical folds (Ago et al., 1991, Eriksson et al., 1991, 1993; Zhang et al., 1991; Zhu et al., 1991). In this paper, the high-resolution NMR solution structure of FGF-2 has been compared to the 1.9 Å X-ray structure of C78S,C96S-FGF-2 by Zhu et al. (1991). The

Table 4: Number of Violations Exhibited by the X-ray Structure of FGF-2 with Respect to the Experimental NMR Interproton Distance and Torsion Angle Restraints[a]

	(A) Number of Violations in Interproton Distance Restraints					
	0.1−0.3 Å	0.3−0.5 Å	0.5−1.0 Å	1.0−2.0 Å	2.0−5.0 Å	>5.0 Å
all (2118)	34	26	37	45	42	0
interresidue sequential ($\|i-j\|=i$) (472)	2	2	7	8	2	0
interresidue short range ($1<\|i-j\|\leq 5$) (237)	0	4	5	6	8	0
interresidue long range ($\|i-j\|>5$) (854)	20	9	20	27	32	0
intraresidue (505)	8	11	4	4	0	0
H-bonds (50)	4	0	1	0	0	0

	(B) Violations in Torsion Angle Restraints			
	10−30°	30−60°	60−120°	>120°
all (309)	24	4	6	7
ϕ (111)	9	0	0	0
ψ (95)	9	2	0	0
χ_1 (76)	5	1	5	0
χ_2 (27)	1	1	1	7

[a] The X-ray structure of FGF-2 is the 1.9 Å resolution X-ray structure of Zhu et al. (1991). Residues 1−27 and 153−155 are not present, and residues 28, 55, 65, 67−69, 87, 85, 99, 119, 129, 133, and 144 have disordered side chains and only contain backbone atoms in the X-ray structure (residue numbering was corrected for the additional eight amino acids in the NMR sequence). The total number of interproton distance and torsion angle restraints in each category is given in parentheses.

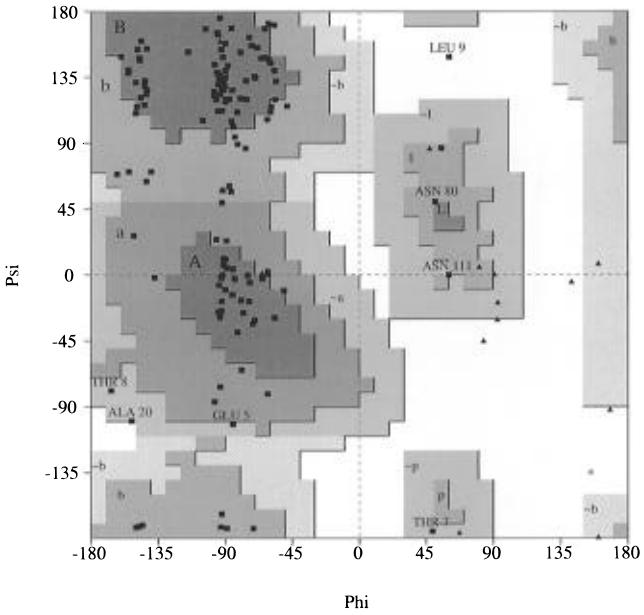

FIGURE 4: Ramachandran ϕ, ψ plot for the restrained minimized mean structure, $\overline{(SA)}_r$, of FGF-2. The different regions of the Ramachandran plot are represented by levels of shading (from dark gray to white: most favorable, allowed, generously allowed, and disallowed). The glycine residues are represented by triangles. The asparagine residues lying in the positive ϕ region of the plot and residues from the disordered N-terminal region of the protein which occur in disallowed or generously allowed regions are labeled. This plot was generated by the PROCHECk program (Laskowsky et al., 1993).

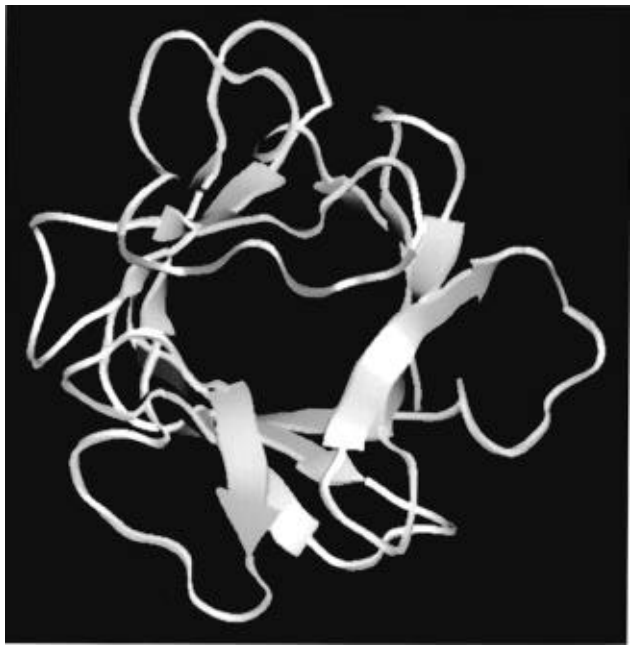

FIGURE 5: Ribbon drawing of the restrained minimized mean structure, $\overline{(SA)}_r$, of FGF-2. The 11 β-strands are shown in yellow, and the helix-like region is shown in blue. The model was generated with Quanta 4.1 (Molecular Simulations, Inc., San Diego).

superposition of the backbone atoms of the restrained minimized mean, $\overline{(SA)}_r$, NMR structure of FGF-2 with the X-ray structure is shown in Figure 9 with a plot of the backbone rms difference as a function of residue. Clearly the two structures are very similar, as evident by the relatively small rms difference between the two structures. For residues 29−152, the atomic rms difference between the restrained minimized mean NMR structure, $\overline{(SA)}_r$, and the X-ray structure is 0.94 Å for the backbone atoms and 1.41 Å for all atoms (Table 3). When only residues involved in secondary structure are considered, these values drop to 0.78 and 1.24 Å, respectively. The only significant differences between the structures appear to be in the loop regions, particularly residues 64, 67−69, 108−111, and 141−142. Mobility in solution and crystal packing are likely to be major contributors to these differences, as evident by the disordered side chains for residues 65, 67−69, and 144 in the X-ray structure.

While the overall folds of the FGF-2 NMR and X-ray structures are quite similar, there clearly are local differences between the structures as indicated by the high values of the NOE and torsion angle restraint energies (Table 2) and by the number of interproton distance and torsion angle violations greater than 2 Å and 60°, respectively, exhibited by the X-ray structure (Table 4). A significant number of the larger violations can be attributed to different χ rotamers. There are a total of six residues between the NMR and X-ray structures that have distinctly different χ_1 rotamers, and nine residues that have distinctly different χ_2 rotamers. Most of the χ_2 rotamer differences are attributed to aromatic residues where differentiating between either the +90° or −90°

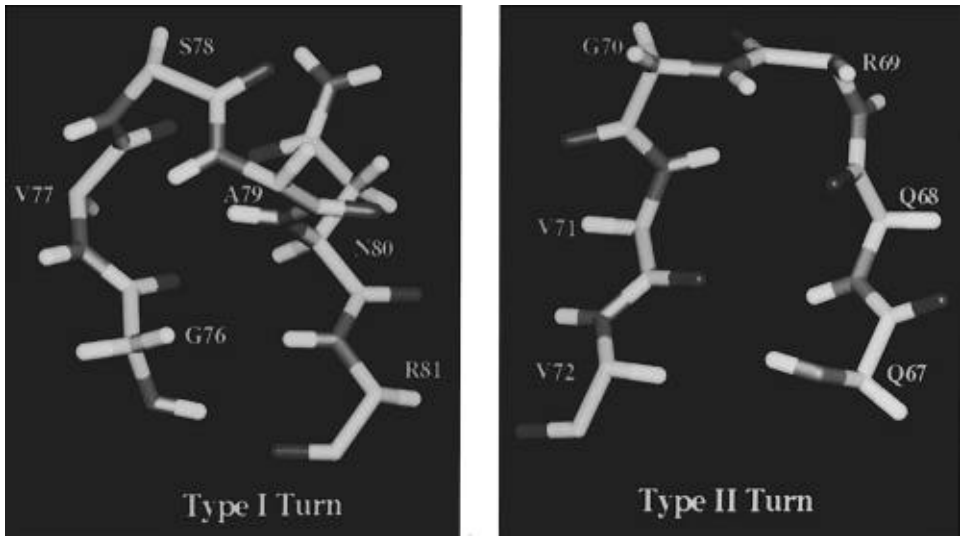

FIGURE 6: Two expanded regions of the backbone (N, Cα, C, O) atoms of the restrained minimized mean structure, $(\overline{SA})_r$, of FGF-2 corresponding to the type II reverse turn between β-strands II and III and the type I reverse turn between β-strands IV and V. A type II reverse turn is characterized by a Gly at position $i + 2$ with a positive ϕ torsion angle and very distinct ϕ and ψ torsion angles from the residue at position $i + 1$. A type I reverse turn is a distorted 3_{10}-helix. Both Gly 70 and Asn 80 adopt a positive ϕ torsion angle. The side chain for Asn 80 is shown.

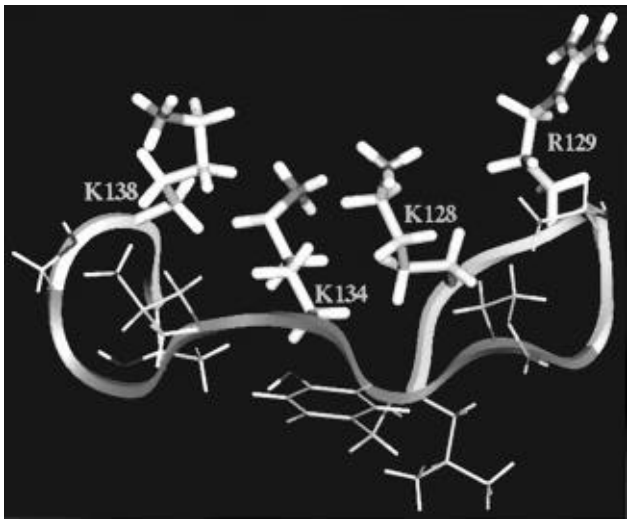

FIGURE 7: Expanded region of the backbone (N, Cα, C, O) atoms of the restrained minimized mean structure, $(\overline{SA})_r$, of FGF-2 corresponding to the primary heparin binding site (residues 128−138). The side chains for residues K128, R129, K134, and K138 which have been identified as part of the heparin binding domain of FGF-2 (Li et al., 1994; Thompson et al., 1994) are shown. The backbone atoms for residues 131−136 which adopt a helix-like conformation are colored purple.

torsion angle in an X-ray structure is not readily apparent. This results in artificially large NOE and torsion angle restraint energies for the X-ray structure. Therefore, the X-ray structure was modified such that the Phe and Tyr χ_2 rotamers were consistent with the NMR structure. The NOE and torsion angle restraint energies in Table 2 reflect these changes. Most of the χ_1 rotamer differences are residues in loop regions where a rotamer change would not have a significant effect on the local structure. Similarly, the significant backbone ϕ and ψ restraint violations seen in the X-ray structure are in loop regions and can be easily attributed to the difference between an average NMR structure and an X-ray structure corresponding to a particular "frozen-out" conformation. Therefore, these observed differences between the X-ray and solution NMR structures are probably of little significance.

It is important to point out that, from an energetic viewpoint, the value of the Lennard Jones−van der Waals energy is significantly less negative for the crystal structure (−280 kcal mol^{-1}) than for the NMR structure (−513 ± 13 kcal mol^{-1}) while there is no significant difference in the values of the solvation free energy of folding. It is not readily apparent what the source of this energy difference is between the two structures since the overall fold is quite similar. It is plausible that the difference could be attributed to a number of small poor nonbonded contacts resulting from slightly skewed χ rotamers caused by crystal packing and the sum of these small errors might account for the overall large energy difference between the two structures.

There is, however, one *descriptive* difference between the solution NMR structure and the X-ray structures of FGF-2. The X-ray structures describe FGF-2 as being composed of 12 β-strands. This was based primarily on the observation that FGF-2 is a structural homolog of interleukin 1β (IL-1β) (Eriksson et al., 1991; Zhang et al., 1991; Zhu et al., 1991), and the assignment of the 12 β-strands in the FGF-2 X-ray structures was inferred from the alignment with IL-1β. Eriksson et al. (1991) noted that strand XI did not meet the Kabsch and Sander criteria for β-sheet strands (Kabsch et al., 1983) but that its location correlated with the β-strand framework from the IL-1β structures. It is clearly evident that residues 131−136, which would correspond to β-strand XI in IL-1β, are helix-like in the FGF-2 structure (Figure 7) (Moy et al., 1995). The helix-like nature of residues 131−136 is evident by small $^3J_{HN\alpha}$ coupling constants for Gly 131, Tyr 133, and Leu 135 in addition to typical sequential NOEs associated with helical regions ($d_{NN(i,i+1)}$, $d_{NN(i,i+2)}$, and $d_{\alpha N(i,i+1)}$) and the lack of across-strand NOEs for a β-strand region.

FGF-2 Heparin Binding. The biological activity of FGF-2 is dependent on its ability to bind heparin. The heparin binding site has been identified by site-directed mutagenesis (Li et al., 1994; Thompson et al., 1994) and by the recent X-ray structure of FGF-2 heparin complexes (Faham et al., 1996). The heparin binding site on FGF-2 is a highly positive charged environment as evident by the electrostatic map of the FGF-2 surface (Figure 10) using the program

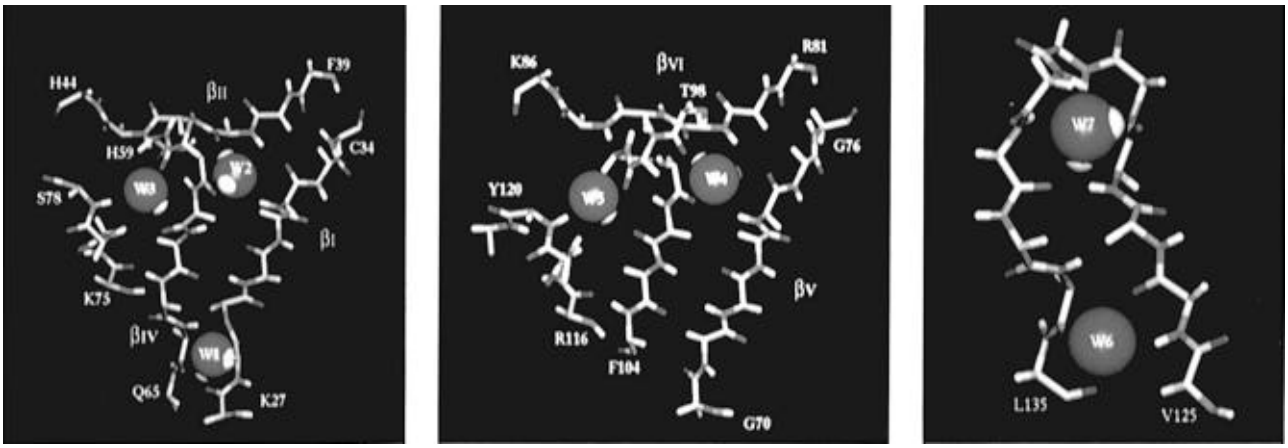

FIGURE 8: Three expanded regions of the backbone (N, Cα, C, O) atoms of the restrained minimized mean structure, $(\overline{SA})_r$, of FGF-2 together with the approximate locations of the seven bound water molecules.

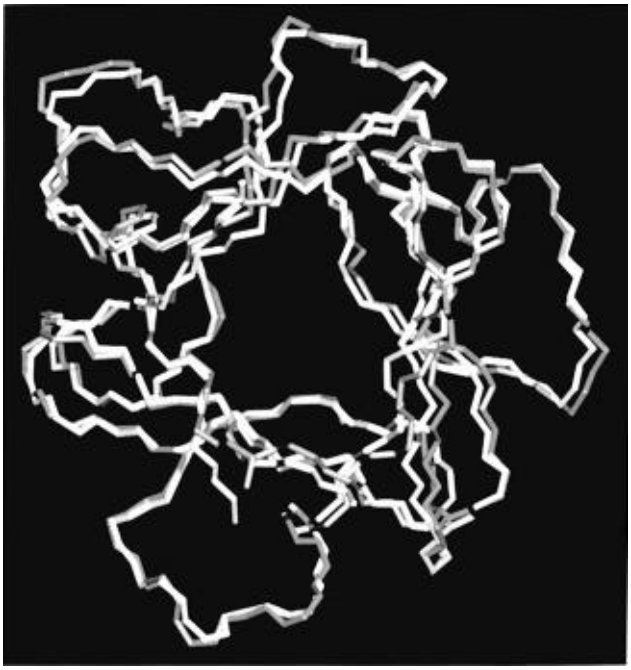

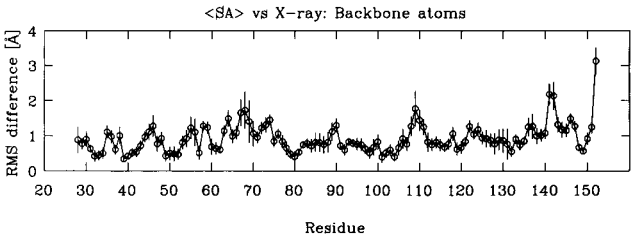

FIGURE 9: Best fit superposition of the backbone (N, Cα, C) atoms of the restrained minimized mean NMR (blue) structure, $(\overline{SA})_r$, and the X-ray (yellow) structure of FGF-2 for residues 29−152 (top). Backbone (N, Cα, C, O) atomic rms differences between the 30 simulated annealing structures and the X-ray structure as a function of residue number (bottom). The circles represent the average value at each residue, and the error bars indicate the standard deviation of these values. The X-ray structure is that of Zhu et al. (1991).

GRASP (Nicholls et al., 1993). The X-ray structures of the FGF-2−heparin complex (Faham et al., 1996) and the FGF-2−SOS complex (Xu et al., 1996) indicate that a primary mode of binding is through the formation of salt bridges between the sulfate groups on the ligand and the Lys $N\zeta H^{3+}$ and Arg guanidinium group on FGF-2. This interaction occurs without an induced conformational change in the FGF-2 structure (Faham et al., 1996; Xu et al., 1996). It is

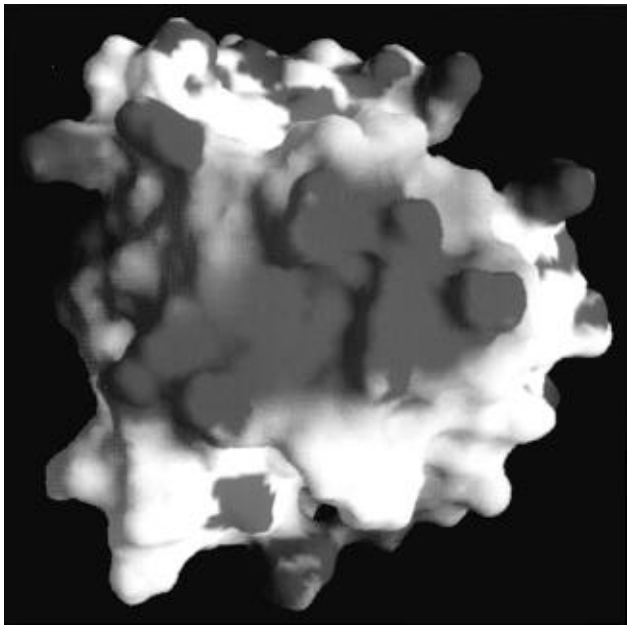

FIGURE 10: Electrostatic surface of the restrained minimized mean structure, $(\overline{SA})_r$, of FGF-2 for residues 29−152 generated using the program GRASP (Nicholls et al., 1993). Blue and red indicate positively charged and negatively charged surfaces, respectively. The highly charged positive surface corresponds to the heparin binding domain of FGF-2.

also interesting to note that two of the seven detected bound waters in the FGF-2 NMR structure occur in this heparin binding region and further stabilize the local structure (Figure 8). Since residues 131−136 compose part of the FGF-2 heparin binding site, the fact that these residues adopt a helix-like secondary structure in FGF-2 instead of the β-strand in Il-1β is probably crucial for the proper orientation of the Arg and Lys side chains to form the required salt bridges with the heparin ligand (Margalit et al., 1993). The proper alignment of FGF-2 side chains for binding with the heparin ligand would clearly play a significant and positive role in the overall energetics of the complex and add to the stability of the FGF-2−heparin interaction. The high-resolution NMR structure of FGF-2 provides the initial information necessary to further investigate the interaction of heparin with FGF-2 and its role in initiating FGF-2 receptor binding.

REFERENCES

Ago, H., Kitagawa, Y., Fujishima, A., Matsuura, Y., & Katsube, Y. (1991) *J. Biochem. 110*, 360−363.

Archer, S. J., Ikura, M., Torchia, D. A., & Bax, A. (1991) *J. Magn. Reson. 95*, 636-641.
Baird, A., & Bohlen, P. (1990) Peptide Growth Factors and their Receptors. In *Handbook of Experimental Pharmacology* (Sporn, M., & Roberts, A., Eds.) Vol. 95, pp 369−418, Springer-Verlag, New York.
Basilico, C., & Moscatelli, D. (1992) *Adv. Cancer Res. 59*, 115−165.
Bax, A., Max, D., & Zax, D. (1992) *J. Am. Chem. Soc. 114*, 6924−6925.
Brooks, B. R., Bruccoleri, R. E., Olafson, B. D., States, D. J., Swaminathan, S., & Karplus, M. (1983) *J. Comput. Chem. 4*, 187−217.
Brunger, A. T. (1993) *X-PLOR Version 3.1 Manual*, Yale University, New Haven, CT.
Chiche, L., Gregoret, L. M., Cohen, F. E., & Kollman, P. A. (1990) *Proc. Natl. Acad. Sci. U.S.A. 87*, 3240−3243.
Clore, G. M., & Gronenborn, A. M. (1991) *Science 252*, 1390−1399.
Clore, G. M., & Gronenborn, A. M. (1992) *J. Mol. Biol. 223*, 853−856.
Clore, G. M., Nilges, M., Sukumaran, D. K., Bruenger, A. T., Karplus, M., & Gronenborn, A. M. (1986) *EMBO J. 5*, 2729−2735.
Clore, G. M., Gronenborn, A. M., Nilges, M., & Ryan, C. A. (1987) *Biochemistry 26*, 8012−8023.
Clore, G. M., Bax, A., Wingfield, P. T., & Gronenborn, A. M. (1990a) *Biochemistry 29*, 5671−5676.
Clore, G. M., Appella, E., Yamada, M., Matsushima, K., & Gronenborn, A. M. (1990b) *Biochemistry 29*, 1689−1696.
Delaglio, F., Grzesiek, S., Vuister, G. W., Zhu, G., Pfeifer, J., & Bax, A. (1995) *J. Biomol. NMR 6*, 277−293.
Eisenberg, D., & McLachlan, A. D. (1986) *Nature 319*, 199−203.
Eriksson, A. E., Cousens, L. S., Weaver, L. H., & Matthews, B. W. (1991) *Proc. Natl. Acad. Sci. U.S.A. 88*, 3441−3445.
Eriksson, A. E., Cousens, L. S., & Matthews, B. W. (1993) *Protein Sci. 2*, 1274−1284.
Faham, S., Hileman, R. E., Fromm, J. R., Linhardt, R. J., & Rees, D. C. (1996) *Science 271*, 1116−1120.
Folkman, J., & Klagsbrun, M. (1987) *Science 235*, 442−447.
Forman-Kay, J. D., Clore, G. M., Wingfield, P. T., & Gronenborn, A. M. (1991a) *Biochemistry 30*, 2685−2698.
Forman-Kay, J. D., Gronenborn, A. M., & Wingfield, P. T. (1991b) *J. Mol. Biol. 220*, 209−216.
Garrett, D. S., Powers, R., Gronenborn, A. M., & Clore, G. M. (1991) *J. Magn. Reson. 95*, 214−220.
Grzesiek, S., & Bax, A. (1993) *J. Am. Chem. Soc. 115*, 12593−12594.
Grzesiek, S., Kuboniwa, H., Hinck, A. P., & Bax, A. (1995) *J. Am. Chem. Soc. 117*, 5312−5315.
Ikura, M., Kay, L. E., Tschudin, R., & Bax, A. (1990) *J. Magn. Reson. 86*, 204−209.
Kabsch, W., & Sander, C. (1983) *Biopolymers 22*, 2577−2637.
Kan, M., Wang, F., Xu, J., Crabb, J. W., Hou, J., & McKeehan, W. L. (1993) *Science 259*, 1918−1921.
Kraulis, P. J., Clore, G. M., Nilges, M., Jones, T. A., Pettersson, G., Knowles, J., & Gronenborn, A. M. (1989) *Biochemistry 28*, 7241−7257.
Laskowski, R. A., MacArthur, M. W., Moss, D. S., & Thornton, J. M. (1993) *J. Appl. Crystallogr. 26*, 283−291.
Li, L. Y., Safran, M., Aviezer, D., Boehlen, P., Seddon, A. P., & Yayon, A. (1994) *Biochemistry 33*, 10999−11007.
Margalit, H., Fischer, N., & Ben-Sasson, S. A. (1993) *J. Biol. Chem. 268*, 19228−19231.
Marion, D., Ikura, M., Tschudin, R., & Bax, A. (1989a) *J. Magn. Reson. 85*, 393−399.
Marion, D., Driscoll, P. C., Kay, L. E., Wingfield, P. T., Bax, A., Gronenborn, A. M., & Clore, G. M. (1989b) *Biochemistry 28*, 6150−6156.
Miyamoto, M., Naruo, K.-I., Seko, C., Matsumoto, S., Kondo, T., & Kurokawa, T. (1993) *Mol. Cell. Biol. 13*, 4251−4259.
Moy, F. J., Seddon, A. P., Campbell, E. B., Böhlen, P., & Powers, R. (1995) *J. Biomol. NMR 6*, 245−254.
Moy, F. J., Safran, M., Seddon, A. P., Kitchen, D., Böhlen, P., Aviezer, D., Yayon, A., & Powers, R. (1996) *Nat. Struct. Biol.* (submitted for publication).
Nicholls, A., Sharp, K., & Honig, B. (1991) *Proteins: Struct., Funct., Genet. 4*, 281 ff.
Nilges, M., Clore, G. M., & Gronenborn, A. M. (1988a) *FEBS Lett. 229*, 317−324.
Nilges, M., Gronenborn, A. M., Brunger, A. T., & Clore, G. M. (1988b) *Protein Eng. 2*, 27−38.
Nilges, M., Clore, G. M., & Gronenborn, A. M. (1988c) *FEBS Lett. 239*, 129−136.
Nilges, M., Clore, G. M., & Gronenborn, A. M. (1990) *Biopolymers 29*, 813−822.
Ornitz, D. M., Yayon, A., Flanagan, J. G., Svahn, C. M., Levi, E., & Leder, P. (1992) *Mol. Cell. Biol. 12*, 240−247.
Otting, G., & Wuthrich, K. (1989) *J. Am. Chem. Soc. 111*, 1871−1875.
Pantoliano, M. W., Horlick, R. A., Springer, B. A., Van Dyk, D. E., Tobery, T., Wetmore, D. R., Lear, J. D., Nahapetian, A. T., Bradley, J. D., & Sisk, W. P. (1994) *Biochemistry 33*, 10229−10248.
Piotto, M., Saudek, V., & Sklenar, V. (1992) *J. Biomol. NMR 2*, 661−665.
Powers, R., Gronenborn, A. M., Clore, G. M., & Bax, A. (1991) *J. Magn. Reson. 94*, 209−213.
Powers, R., Garrett, D. S., March, C. J., Frieden, E. A., Gronenborn, A. M., & Clore, G. M. (1993) *Biochemistry 32*, 6744−6762.
Reiland, J., & Rapraeger, A. C. (1993) *J. Cell Sci., 105*, 1085−1093.
Roghani, M., & Moscatelli, D. (1992) *J. Biol. Chem. 267*, 22156−22162.
Seddon, A., Decker, M., Muller, T., Armellino, D., Kovesdi, I., Gluzman, Y., & Bohlen, P. (1991) *Ann. N.Y. Acad. Sci. 638*, 98−108.
Thompson, L. D., Pantoliano, M. W., & Springer, B. A. (1994) *Biochemistry 33*, 3831−3840.
Vuister, G. W., & Bax, A. (1993) *J. Am. Chem. Soc. 115*, 7772−7777.
Vuister, G. W., Delaglio, F., & Bax, A. (1992) *J. Am. Chem. Soc. 114*, 9674−9675.
Wagner, G., Braun, W., Havel, T. F., Schaumann, T., Go, N., & Wuethrich, K. (1987) *J. Mol. Biol. 196*, 611−639.
Williamson, M. P., Havel, T. F., & Wuethrich, K. (1985) *J. Mol. Biol. 182*, 295−315.
Wüthrich, K., Billeter, M., & Braun, W. (1983) *J. Mol. Biol. 169*, 949−961.
Xu, Z., Seddon, A., Kitchen, D., Bohlen, P., & Venkataraghavan, R. (1996) *Structure* (manuscript in preparation).
Yayon, A., Klagsbrun, M., Esko, J. D., Leder, P., & Ornitz, D. M. (1991) *Cell 64*, 841−848.
Zhang, J., Cousens, L. S., Barr, P. J., & Sprang, S. R. (1991) *Proc. Natl. Acad. Sci. U.S.A. 88*, 3446−3450.
Zhu, X., Komiya, H., Chirino, A., Faham, S., Fox, G. M., Arakawa, T., Hsu, B. T., & Rees, D. C. (1991) *Science 251*, 90−93.
Zuiderweg, E. R. P., & Fesik, S. W. (1989) *Biochemistry 28*, 2387−2391.
Zuiderweg, E. R. P., Boelens, R., & Kaptein, R. (1985) *Biopolymers 24*, 601−611.
Zuiderweg, E. R. P., McIntosh, L. P., Dahlquist, F. W., & Fesik, S. W. (1990) *J. Magn. Reson. 86*, 210−216.

BI961260P